RELAP5 ANALYSIS OF TWO-PHASE DECOMPRESSION AND RAREFACTION WAVE PROPAGATION UNDER A TEMPERATURE GRADIENT

Nathan Lafferty, Martin Lopez de Bertodano, Victor H. Ransom

School of Nuclear Engineering, Purdue University, West Lafayette, Indiana 47907-1290

bertodan@purdue.edu

Number of:

Pages 58

Tables 0

Figures 32

Abstract

The capability of RELAP5 to model single and two-phase acoustic wave propagation is demonstrated with the use of fine temporal and spatial discretizations. Two cases were considered: a single phase air shock tube problem was simulated resulting in a shock and a rarefaction wave that lie within 1% error of the analytic solution and pressure oscillations observed by Takeda and Toda in a two-phase decompression experiment in a pipe under a temperature gradient.

Whereas the agreement for the single phase case is excellent, some discrepancies were observed in the two-phase case:

1. Thermal nonequilibrium and the associated delay in the bubble growth were identified as the cause for the dispersion of the rarefaction wave as it becomes trapped inside a two-phase fluid region. The short timescale of the experiment justifies the use of a bubble diameter that is one order of magnitude smaller than the standard RELAP5 predicted bubble diameter, which is calibrated for longer transients.
2. The initial depressurization undershoots seen in the Takeda and Toda experiment was over predicted by the RELAP5 model. Improved agreement with the experiment was obtained by altering the discharge coefficient in the choked flow model to account for uncertainties in the discharge geometry and/or the choked flow model at low pressure.

By adjusting these parameters RELAP5 produced markedly better comparisons with the experimental data. These results illustrate two generic shortcomings of nuclear reactor system codes, i.e. the absence of a dynamic model for the interfacial area concentration

and uncertainty in two-phase choked flow modeling. However, it is remarkable that RELAP5 could predict the complex dynamics of the two-phase acoustic phenomena in the Takeda and Toda experiment in spite of these shortcomings.

Keywords Two phase flow, two-fluid model, pressure waves, choked flow, interfacial area concentration

1 Introduction

Acoustic wave propagation phenomena are of key interest in the field of nuclear reactor safety. To understand the forces on internal reactor components it is necessary to analyze fluid behavior immediately after a postulated LOCA [1]. Such an analysis provides insight into possible structural damage resulting in a failure to maintain core geometry and core cooling.

In the event of a LOCA in a water cooled reactor, the subcooled blowdown process results in the propagation of a rarefaction wave [1]. The wave eventually travels from the point of the break through the coolant piping to the nuclear reactor's core region [2]. Furthermore, a temperature gradient in the core leads to unique behavior of the rarefaction wave. Takeda and Toda show that for a pipe with a temperature gradient, flashing in the hotter section results from the passing of a rarefaction wave with a large enough amplitude; whereas, the colder section, with a lower vapor pressure, remains a subcooled liquid [2]. A large discontinuity in the sound speed is created between the two-phase and single-phase regions serving as a reflective surface and creating the observed pressure oscillations [2].

Edwards and O'Brien (1970) compared numerical simulations which track the initial rarefaction wave and related void formation following the bursting of a pressurized horizontal subcooled pipe of constant temperature with experimental results [1]. Later, Takeda and Toda (1979) experimentally observed the pressure behavior in a vertical pipe under a temperature gradient and analyzed it with simple equilibrium and nonequilibrium wave propagation models [2] . In both cases the authors used their own computational codes for simulating the blowdown experiments and tracking the pressure waves [1],[2].

The data from Edwards and O'Brian has been used to validate the two-fluid model in the RELAP5 computer code [3]. The data from Takeda and Toda, however, contains wave propagation in both single and two-phase fluids and has never been compared with a RELAP5 simulation.

The RELAP5 computer code widely used in nuclear reactor transient analysis employs a two fluid model consisting of the mass, momentum, and energy conservation equations for each phase solved using a semi-implicit finite-difference technique [3]. The ability of RELAP5 to solve the single-phase and two-phase wave equations is further revealed in a simulation of a two-phase shock tube and water hammer analysis benchmarked with experimental data carried out by Tiselj and Cerne [4]. Tiselj and Cerne have demonstrated that RELAP5 is capable of tracking acoustic waves with almost second-order accuracy with the use of small time steps [4].

This work consists of two parts: First, the application of RELAP5/MOD3.3 Patch03 to model an air filled shock tube (i.e. Riemann's problem) at very small time steps and a refined grid. Secondly, the RELAP5 simulation of the experiment carried out by Takeda and Toda.

2 Air Shock Tube

A shock tube was investigated using the RELAP5/MOD3.3 code to validate it for single-phase wave propagation. The corresponding simplified one-dimensional single-phase continuity and momentum equations are listed below [4]:

$$\begin{aligned} &\frac{\partial \rho}{\partial t}+\frac{\partial \rho v}{\partial x}=0 \\ &\rho \frac{\partial v}{\partial t}+\frac{\rho}{2}\frac{\partial v^2}{\partial x}+\frac{\partial p}{\partial x}=0 \end{aligned} \tag{1}$$

Tiselj and Cerne derived the following simplified single-phase acoustic wave equations

$$\begin{aligned} &\frac{\partial \rho}{\partial t}+\rho \frac{\partial v}{\partial x}=0 \\ &\rho \frac{\partial v}{\partial t}+\frac{\partial p}{\partial x}=0 \end{aligned} \tag{2}$$

assuming a negligible fluid velocity and $\delta\rho/\rho$ ratio [4]. These are reasonable assumptions due to the very small density fluctuations and fluid velocity relative to the sonic velocity. Tiselj and Cerne show that when Eqs. (2) are discretized following the RELAP5 procedure, the first order spatial truncation errors vanish [4]

The shock tube model consists of stagnant air separated by a diaphragm shown in Fig. 1. Gas 3 on the left side of the diaphragm is initially at a higher pressure than gas 1. In order to allow an analytical solution the air on each side of the diaphragm has initially the same temperature. The diaphragm is broken creating a right-traveling shock wave and a left-traveling rarefaction wave as shown. The velocity of fluids states 2 and 4 are the same. No entropy change between fluid states 3 and 4 takes place, and entropy increases across the shock from 1 to 2, so the temperatures in fluid states 2 and 4 are different [5].

A 9.9 meter pipe is divided into 99 nodes, each one 0.1 m long. The cross sectional area of the pipe is 0.00456 m^2 (3 inch inner diameter). Tiselj and Cerne recommend short time steps, $\Delta t \approx 0.01\frac{\Delta x}{c}$, in order to trace acoustic waves with almost second-order accuracy [4]. Therefore, the time step was chosen to produce a value of about 0.01 for the acoustic Courant Number. The gas used for this experiment is air at 297 K. Gas 3, to the left of the diaphragm, is initialized at 2 MPa and Gas 1, to the right, is at 1 MPa. The pipe is adiabatic.

Fig. 2 shows the progression of the shock and rarefaction waves in the tube. The dense nodalization and small time step produce results matching the analytic solution. For the analytic solution the air is assumed a perfect gas, which is valid since the ratio of the temperature to the critical temperature is greater than two, and the specific heats are approximately constant due to the minor temperature fluctuations. The pressure of gas 2 calculated by RELAP5 is 1.406 MPa and when compared with the analytic solution [5] of 1.402 MPa produces only 0.29% relative error. Selecting the RELAP5 10 ms data, the shock wave velocity is 400 m/s and has an error of 0.24%. The velocity of gas 2 taken from RELAP5 is 84.12 m/s, and has a 1.7% relative error compared to the analytic value of 84.49 m/s. The behavior of the pressure wave also matches what is predicted. The shock wave has a relatively steep slope that stays steep, while the rarefaction wave spreads as it propagates [5]. The nonphysical numerical oscillations are a byproduct of the reduced time step. Increasing the time step reduces the numerical oscillations but diffuses the steep pressure gradients [4].

3 Blowdown Under Temperature Gradient

Takeda and Toda measured pressure oscillations during the decompression of a vertical pipe with a temperature gradient [2]. The pipe may be divided into a two-phase region at the top and a subcooled region in the rest of the pipe.

The RELAP5 one-dimensional mass and momentum conservation equations equivalent to Eqs. (1) governing wave propagation in the two-phase region are given below [3],[6].

Conservation of mass:

$$\begin{aligned} \frac{\partial}{\partial t}(\alpha_g \rho_g) + \frac{\partial}{\partial x}(\alpha_g \rho_g v_g) &= \Gamma_g \\ \frac{\partial}{\partial t}(\alpha_f \rho_f) + \frac{\partial}{\partial x}(\alpha_f \rho_f v_f) &= -\Gamma_g \end{aligned} \tag{3}$$

Conservation of momentum:

$$\begin{aligned} \frac{\partial(\alpha_g \rho_g v_g)}{\partial t} + v_g \frac{\partial(\alpha_g \rho_g v_g)}{\partial x} &= -\alpha_g \frac{\partial P}{\partial x} + \alpha_g \rho_g g - F_{wg} - F_I + \Gamma_g (v_I - v_g) \\ \frac{\partial(\alpha_f \rho_f v_f)}{\partial t} + v_f \frac{\partial(\alpha_f \rho_f v_f)}{\partial x} &= -\alpha_f \frac{\partial P}{\partial x} + \alpha_f \rho_f g - F_{wf} + F_I - \Gamma_g (v_I - v_f) \end{aligned} \tag{4}$$

Where α, ρ, and v are the time and space averaged void fraction, density, and velocity, and the g and f subscripts specify vapor and liquid respectively [6]. Γ_g is the vapor generation. P is the pressure averaged between the two phases [6]. The volumetric wall shear forces experienced by the liquid and vapor are F_{wf} and F_{wg}, respectively [6]. F_I is the volumetric interfacial drag and v_I is the interfacial velocity in the interfacial

momentum transfer terms [6]. Eqs. (3) and (4) describe the wave propagation in a two-phase medium. In addition, the two-phase energy conservation equations in RELAP5 are required in order to model the vapor generation that occurs during the depressurization process [3].

Conservation of energy:

$$\begin{aligned}
&\frac{\partial}{\partial t}(\alpha_g \rho_g u_g) + \frac{\partial}{\partial x}(\alpha_g \rho_g u_g v_g) = -P\frac{\partial \alpha_g}{\partial t} - P\frac{\partial}{\partial x}(\alpha_g v_g) + Q_{ig} + \Gamma_{ig} h_g^* \\
&\frac{\partial}{\partial t}(\alpha_f \rho_f u_f) + \frac{\partial}{\partial x}(\alpha_f \rho_f u_f v_f) = -P\frac{\partial \alpha_f}{\partial t} - P\frac{\partial}{\partial x}(\alpha_f v_f) + Q_{if} - \Gamma_{ig} h_f^*
\end{aligned} \tag{5}$$

The specific internal energy is represented by u, Q_{ig} and Q_{if} are the interfacial heat transfer terms, Γ_{ig} is the vapor generation resulting from interfacial energy exchange, and h_g^* and h_f^* are the corresponding phasic enthalpies associated with interphase mass transfer[3]. The effects of wall heat transfer and the energy dissipation caused by friction are negligible and omitted in Eqs. (5).

A RELAP5 model was developed from Takeda and Toda's experimental setup [2]. The water filled pipe has a 53.5 mm inner diameter, a 3.2 m length, and is pressurized to 0.855 MPa measured at the top. It contains 99 nodes, each 3.23 cm in length. Fig. 3 shows a diagram of the RELAP5 model. The experimental data [2] was taken at pressure transducers (PT) 3, 4, and 5 which are located at a distance from the break of 0.444, 1.20, and 2.20 m respectively. The volume labeled BC is a time dependent volume representing the atmospheric boundary conditions. The junction representing the break orifice is 15 mm in diameter and is positioned at the top of the test section. It is modeled with an abrupt area change so the code calculates flow losses through the break [3]. A linear temperature distribution is established in the pipe such

that the temperature at the base of the pipe is 283.7 K and the temperature at the top is 437.9 K. This temperature distribution produced the greatest pressure oscillations out of the many temperature distributions tested experimentally by Takeda and Toda and will therefore be used in this analysis. Fig. 3 shows the vapor pressure of the water in the pipe based on the initial temperature distribution. The vapor pressure is greatest at the top of the pipe near the postulated break with a value of 0.696 MPa.

Spatial convergence was checked by comparing the 99 node model with a finer 297 node model. Both models produced matching results, therefore the 99 node model was used for further investigations. The effects of adding a heat structure were also investigated and proved negligible, thus confirming the adiabatic assumption. The Ransom-Trapp critical flow model was adopted as it captured the experimental pressure behavior more accurately. A 550 microsecond delay time was applied to the simulated break in order to match the delay in the experimental results.

3.1 Thermal Equilibrium Assumption

The RELAP5 thermal equilibrium option was used in order to provide insight into the depressurization and wave propagation with simplified fluid assumptions. Figs. 4-6 show that the results converge as the time step decreases. The acoustic Courant Numbers 1, 0.1, and 0.01 correspond to the a time step value of $\Delta t = \frac{\Delta x}{c}$, $\Delta t = 0.1\frac{\Delta x}{c}$, and $\Delta t = 0.01\frac{\Delta x}{c}$ respectively. It is seen that an acoustic Courant Number of 0.1 produces converged results with minimal numerical oscillation that require the least computational effort.

The RELAP5 simulation with the thermal equilibrium model overpredicts the pressure when compared with the experimental data (Figs. 4-6). A physical explanation for the pressure calculated with the equilibrium model is that immediately following the pipe rupture, the efflux of fluid through the break leads to a sudden pressure drop to the vapor pressure, 0.696 MPa, at the top of the pipe. Due to the assumption of instantaneous heat transfer between the vapor and liquid, some fluid immediately flashes to steam and a region of low void is formed near the break. This region is the thin black strip at the top shown in Fig. 7 and does not penetrate deep into the pipe. This is because no pressure undershoot occurs. The two-phase region near the pipe break lowers the local speed of sound to approximately 50 m/s as shown in Fig. 7 and the flow at the break is choked [7]. The pressure in the pipe then stabilizes at the vapor pressure of the fluid and sets the amplitude of the rarefaction wave. The rarefaction wave travels down the pipe, reflects off the closed end as another rarefaction wave of equal strength propagates back toward the top of the pipe where the two-phase region exists, as seen in Fig. 8. Fig. 8 shows a 2D shaded contour plot of the pressure. A line separating to regions of uniform color represents a characteristic line and displays the propagation of the wave front.

The rarefaction wave is reflected by the discontinuity in the sound speed, from 1500 m/s to 50 m/s, at the boundary between the single and two-phase flow regions. According to wave propagation theory the reflection and transmission of a wave at an interface with a change in the sound speed [8] is given by

$$A_R = \frac{\mu - 1}{\mu + 1} A_I$$
$$A_T = \frac{2\mu}{\mu + 1} A_I \tag{6}$$
$$\mu = \frac{c_T}{c_I}$$

Where A_R, A_T, and A_I are the amplitude of the reflected, transmitted and reflected wave, respectively. The speed of sound on the transmission side of the interface is c_T and on the incident side is c_I [8]. Due to the very small value for the speed of sound in the two-phase mixture compared to the speed of sound of the liquid, μ is approximately zero. Therefore, the amplitude of the reflected wave is nearly the same as the incident wave and opposite in sign, which matches the wave behavior simulated by RELAP5 at the two-phase interface described above. The two-phase region can also be viewed as a constant pressure boundary because as the wave interacts with it, the two-phase region's smaller bulk modulus volumetrically adjusts with little change in pressure. This will cause the wave to be reflected in an opposite sense with a magnitude similar to that of the incident wave.

Fig. 9 shows the interaction of the doubled rarefaction wave with the vapor pressure established by the temperature gradient. The moment the local pressure drops to the vapor pressure, due to the progression of the rarefaction wave, vaporization occurs and the pressure stays at saturation value without dropping below it. The brief extension of the two-phase region during this process is visible in Fig 7 at around 5 ms. The wave then reflects off the already established two-phase region collapsing the newly voided region and progresses back down the pipe as a compression wave. Minor dispersion, diffusion, and dissipation of the wave is seen in Fig. 8. By understanding the simplified

case of thermal equilibrium, insight is obtained into the importance of nonequilibrium effects caused by interfacial energy transfer and delayed nucleation.

3.2 Default Thermal Nonequilibrium

Using the default thermal nonequilibrium model in RELAP5, Figs. 10-12 show the convergence by reducing the time step compared with the experimental data. As the time step decreases the pressure gradients steepen; however, with a very small time step nonphysical numerical oscillations emerge at the pressure discontinuities. Reducing the time step also results in a more accurate integration of the interphase mass, energy, and momentum terms [4].

The default simulation results match qualitatively the experimental behavior of the rarefaction wave better than the equilibrium model. However, RELAP5 predicted a larger pressure undershoot as seen at the initial pressure drop, around 1 ms, in Fig. 10 and continued to underpredict the pressure throughout the remaining 20 ms at PT 3. Figs. 11 and 12 show a similar trend. The steeper pressure drop curve predicted by RELAP5 denotes an overestimation of the pressure drop rate compared to the experimental data. RELAP5 calculates the propagation velocities of the wave through the subcooled fluid with great accuracy. The default simulation results show the attenuation of the wave amplitude and dispersion of the wave during propagation to be slightly exaggerated compared with the experimental data.

Fig. 13 displays the pressure from the default simulation along the pipe length for the duration of the transient in a three-dimensional plot. The experimental data from Takeda and Toda is superimposed on the plot at the locations where the three pressure

transducers reside. The initial pressure drop down to about 0.55 MPa is shown, with a 0.15 MPa pressure undershoot, as the rarefaction wave travels down the pipe. The wave is reflected off the closed end in a like sense, and travels back toward the top of the pipe as another rarefaction wave with an amplitude similar to that of the incident wave. Fig. 14 displays a contour plot that shows the soundspeed distribution in the pipe for 20 ms. Fig. 15 provides a more detailed view of the void fraction at around 5 ms. Fig. 16 displays a contour plot for the pressure showing the wave characteristics as it reflects off the solid boundary at the bottom and the two-phase region at the top of the pipe.

At around 5 ms, as the doubled rarefaction wave travels to the top of the pipe, the region of two-phase flow is suddenly extended from about 0.2 m to about 0.7 m down into the pipe, as shown in Figs. 14 and 15. This occurs due to the interaction of the doubled rarefaction wave with the decreasing vapor pressure caused by the initial temperature gradient shown in Fig. 3. Fig. 17 illustrates the conditions in the pipe as the doubled rarefaction wave travels toward the already established two-phase region. When the rupture occurs, the pressure at the very top of the pipe drops below saturation due to nonequilibrium effects and delay in nucleation. Upon nucleation the pressure is maintained below the vapor pressure by the amount $p_{undershoot}$, and this pressure drop propagates down the pipe in the form of a decompression or rarefaction wave. Voiding occurs due to the tension on the fluid as the rarefaction wave propagates, and the two-phase region extends to the point where the vapor pressure equals the pressure of the expanded fluid left behind the rarefaction wave front. The rarefaction wave reflects off the solid boundary at the bottom of the pipe and doubles back toward the top of the pipe. Once the reflected rarefaction wave causes the local pressure to drop below the vapor

pressure, the fluid is put in tension $p_{tension}$, and voiding begins as shown in Fig. 18. The value of $p_{tension}$ is determined by the delay in nucleation and nonequilibrium effects. Figs. 15 and 19 demonstrate the ability of RELAP5 to simulate the above mentioned phenomena. In Fig. 19 the dotted line represents the vapor pressure, the solid line the pressure distribution and rarefaction wave, and the dashed grey line shows the boundary between the two-phase and single-phase fluid regions. The figure taken at 4.4563 ms shows that a separated region of two-phase fluid forms, surrounded on both sides by single-phase fluid, resembling Fig. 18. The rarefaction wave is then reflected off the initial two-phase region, created by the passing of the first rarefaction wave, but it is trapped in a two-phase region that it formed in its wake that extends to 0.7 m. Once caught, the wave then disperses because it takes a long time to pass through the two-phase region. The figure at 4.5705 ms demonstrates the nonequilibrium and delayed nucleation effects as the fluid pressure drops below the vapor pressure. The dispersion of the wave is visible in Figs. 13 and 16. Particularly in Fig. 16, the pressure discontinuity is initially abrupt, but after the interaction with the two-phase region at 5 ms, the pressure discontinuity spreads out as shown by the blurring of the color contours. Fig. 16 shows the effects of dispersion toward the end of the transient as the waves interact causing bifurcation. The dissipation of the wave amplitude is also significant.

3.3 Discussion

3.3.1 Choked Flow Model

The overprediction of the initial pressure undershoot seen in the RELAP5 default simulation provides a basis for an investigation into the choked flow model. A subcooled discharge coefficient for the Ransom-Trapp critical flow model [9] may be adjusted in order to adjust the pressure undershoot. The discharge coefficient is a user-specified parameter to correct for uncertainties caused by break geometries and the critical flow model. It is multiplied by the throat area and is equivalent to adjusting the break area. It is known that for subcooled conditions the Ransom-Trapp critical flow model calculates too large of a break flow [3]. For an orifice geometry, which is used as the break in the Takeda and Toda experiment, the discharge coefficient is generally reduced [3]. Furthermore, the break in the Takeda and Toda experiment involved the rupture of a Mylar paper disk, and fragments could remain and obstruct the flow resulting in a smaller break area. Therefore the reduction of the subcooled discharge coefficient is justifiable.

Figs. 20-22 show the effect of the subcooled discharge coefficient at PT 3, 4 and 5. The discharge coefficient values of 0.25, 0.5, 0.75, and 1.0 (default simulation) are compared with the experimental data. It is shown that a discharge coefficient of 0.5 produces the best agreement with the pressure undershoot observed in the experiment. In doing so, however, the amplitude of the reflected rarefaction wave is reduced as shown most notably in Fig. 22. After reflecting off the two-phase region at around 5 ms, the compression wave's amplitude is also reduced. Although the discharge coefficient can set a pressure undershoot that matches the experimental data, the pressure drop rate remains unchanged so the initial rarefaction wave still has a steeper slope than the slope

seen experimentally. This discrepancy may be caused by error in the experimental data. The possibility of a delay in the response of the pressure transducer measuring system must be considered.

3.3.2 Interfacial Heat Transfer

A thorough study of the physical mechanism that controls bubble formation and growth is needed in order to determine the bulk interfacial heat transfer model. Increased bubble growth would result in a pressure increase tending toward equilibrium at a faster rate. During the entire depressurization period under investigation, 20 ms, the fluid remains in the bubbly flow regime. Also, due to the pressure undershoot the fluid is a superheated liquid resulting in vaporization and heat transfer from the fluid to the bubble interface as shown in Fig. 23. Therefore, the corresponding liquid interfacial heat transfer is investigated for the case of a bubbly superheated liquid. The liquid interfacial heat transfer term [3] shown in Eqs. (5) is calculated as

$$Q_{if} = h_{if} a_{gf} (T^s - T_f) \tag{7}$$

The variable T^s denotes saturation temperature, T_f *is* the liquid temperature, h_{if} is the liquid interfacial heat transfer coefficient, and a_{gf} is the interfacial area per unit volume. The volumetric mass vaporization rate at the interface [3] assuming negligible heat transfer from the vapor to the bubble interface is

$$\Gamma_{ig} = -\left[\frac{h_{if} a_{gf} (T^s - T_f)}{h_g^s - h_f} \right] \tag{8}$$

The underlying parameter to be adjusted that dictates the energy transfer between the phases, hence the rate of vaporization, is the interfacial area per unit volume [3]. For spherical bubbles it is given by

$$a_{gf} = \frac{6.0\alpha_{bub}}{d_b} \tag{9}$$

where α_{bub} is calculated to be

$$\alpha_{bub} = \max(\alpha_g, 10^{-5}) \tag{10}$$

The Sauter-mean bubble diameter, d_b, is essential in calculating all energy, mass, and momentum transfer that occur between the two phases. As Eqn (9) shows, the bubble diameter determines the interfacial area concentration, a_{gf}. In RELAP5/MOD3.3 Patch03 the bubble diameter is calculated as a function of the Laplace Length [10],[11]

$$d_b = 2L_o \tag{11}$$

where the Laplace Length can be found by

$$L_o = \sqrt{\frac{\sigma}{g(\rho_f - \rho_g)}} \tag{12}$$

The bubble diameter is restricted by the bounds 0.1 mm $\leq d_b \leq 0.9d_h$, where d_h is the volume hydraulic diameter [3].

The bubble diameter was adjusted to correct the underprediction of the pressure using the RELAP5 default simulation. By reducing the bubble diameter, the interfacial area concentration will increase and thus the interfacial heat transfer will increase. This will then cause more vaporization and a slight increase in the pressure. This adjustment was performed by multiplying the Laplace Length, or bubble radius, by a factor. Figs. 24-26 show the effect of multiplying the Laplace Length by a factor of 0.001, 0.1, 0.25, and 1.0 (default simulation) compared with the experimental results. The figures show that as the bubble diameter is reduced, the interfacial area and interfacial heat transfer is increased, and the pressure in the pipe rises. It is important to note that the bubble

diameter has no effect on the pressure undershoot during the initial depressurization. That value is determined by the choked flow model. The explanation for the ramp in pressure after the pressure undershoot, around 1 ms, shown in Figs. 24-26 is that the upper pipe section is initially in tension, see Fig. 23, and is vaporizing faster at that location due to the increased interfacial heat transfer, which then causes the pressure to increase relatively slowly toward equilibrium.

The Laplace Length, hence bubble radius, at various positions in the pipe calculated from the RELAP5 default simulation is around 2.3 mm. RELAP5was designed for transients with much longer durations using steady state two-phase flow regimes. In the present case, the actual bubble radius should be smaller due to the very short time duration of the experiment. The time dependent size of the bubble is initially inertially controlled [12] and can be modeled with the Rayleigh-Plesset equation [13]. However, after a very short critical time thermal effects limit the bubble growth and Plesset-Zwick theory is added to the Rayleigh-Plesset equation [13]. Using the default simulation fluid conditions near the break, the critical time is calculated to be about 80 nanoseconds. The bubble growth, therefore, is namely restricted by thermal effects for the duration of the experiment. The thermal bubble radius is calculated using the Plesset-Zwick [14] theory

$$R = \frac{1}{2C(1/2)} \frac{\rho_f c_{pf} (T_f - T_{sat})}{\rho_g h_{fg}} (\alpha_f t)^{1/2} \tag{13}$$

where the value of $C(1/2)$ is calculated to be $\frac{\sqrt{3\pi}}{6}$. The constant values of superheat required for the calculation are taken to be the greatest possible values as shown in Fig. 23 and occur at about 6 ms.

A plot of the bubble radius against time is shown in Fig. 27. This plot displays an upper limit for the bubble radius because it is calculated using the greatest superheat value in Fig. 23 at a location near the pipe break where the fluid experiences the greatest tension, and the pressure undershoot is greatest due to the underprediction obtained in the default simulation. Even then, the bubble radius is nearly an order of magnitude less than the 2.3 mm bubble radius used in the RELAP5 simulation. This justifies the use of a 0.1 multiplication factor to be used on the Laplace Length.

3.4 Modified RELAP5 Results

The justification for the use of a 0.5 subcooled discharge coefficient and a reduction in the bubble diameter by a factor of 10 has been given. As Figs. 28-30 demonstrate, the combination of these two changes to the default simulation produce results that match the experimental results better than the default models. The discharge coefficient sets the correct pressure undershoot, whereas, the decrease in bubble diameter causes the pressure in the tube to increase and match the data better. Figs. 31 and 32 show the modified results that lie between the default simulation and equilibrium simulation results, which is where the experimental data reside. Hence, the two key parameters determining the simulation discrepancies have been identified and the justification for adjusting them to give results closer to the experimental data was given.

4 Conclusions

The RELAP5 nuclear safety analysis code is capable of simulating fast transients involving depressurizations and acoustic pressure wave propagation. RELAP5 simulated a gas shock tube and the results were found in close agreement with an analytic solution. Also, using RELAP5 with the default options allowed for the simulation of a two-phase decompression under a temperature gradient. Such a problem requires the solution of the two-fluid wave equation and many constitutive models to account for phase changes, choked flow, and other pertinent phenomena. The experimental results of Takeda and Toda were used as a benchmark and were qualitatively well matched by the RELAP5 results. RELAP5 captured the reflection of the pressure wave off of a sound speed discontinuity between a single-phase and two-phase region. The reflection of the wave off the solid pipe end was also captured.

Two RELAP5 constitutive models that caused discrepancies between the computational and experimental results were identified:

1. The choked flow model used by RELAP5 resulted in RELAP5 overpredicting the pressure undershoot. However, this was resolved by altering the discharge coefficient in the choked flow model to account for uncertainties in the discharge geometry and/or the choked flow model at low pressure.
2. The RELAP5 default simulation also underpredicted the pressure due to the estimation of a bubble diameter that was too large resulting in an underpredicted interfacial heat transfer rate. RELAP5 does not have an interfacial area transport model to capture the dynamics of the bubble size, which is a very significant effect in the present transient. Using the Plesset-Zwick theory for such a fast

transient, the average bubble diameter was shown to be one order of magnitude smaller and the RELAP5 code was adjusted to compute the proper bubble diameter by using a multiplication factor.

With the adjusted choked flow discharge coefficient and bubble diameter the RELAP5 solution was improved and matched the experimental data better than the default models.

The data obtained from the RELAP5 simulation also proved useful in better understanding the physics of the experiment. The cause of the dispersion and dissipation of the wave upon reflecting off the two-phase region was identified to be caused by the wave becoming trapped inside a two-phase flow region. Also, the importance of thermal nonequilibrium and delay in bubble nucleation were made evident by an investigation of the RELAP5 results. Therefore, RELAP5 proved to be useful as a heuristic tool in conjunction with the experimental data.

References

[1] Edwards, A R and O'Brien, T P. *Studies of Phenomena Connected with the Depressurization of Water Reactors.* Journal of the British Nuclear Energy Society, 1970, pp. 125-35.

[2] Takeda, Y and Toda, S. *Pressure Oscillation in Subcooled Decompression under Temperature Gradient.* Journal of Nuclear Science and Technology, 1979, pp. 484-495.

[3] Information Systems Laboratories, Inc. *RELAP5/MOD3.3 CODE MANUALVOLUME I - VIII.* Rockville, MD and Idaho Falls, ID , 2006.

[4] Tiselj, I and Cerne, G. *Some Comments on the Behavior of the RELAP5 Numerical Scheme at Very Small Time Steps,* Nuclear Science and Engineering, 2000, p. 306.

[5] Shapiro, A. *The Dynamics and Thermodynamics of Compressible Fluid Flow, Vol 2.* Ronald Press Co., 1954.

[6] Pokharna, H, Mori, M and Ransom, V. *Regularization of Two-Phase Flow Models: A Comparison of Numerical and Differential Approaches.* Journal of Computational Physics, Vol. 134, 1997, pp. 282-295.

[7] Ivashneva, M, Ivashnyov, O and Smirnov, N. *Slow Waves of Boiling Under Hot Water Depressurization.* Journal of Fluid Mechanics, 2000, pp. 149-180.

[8] Davis, J. *Mathematics of Wave Propagation.* Princeton University Press, 2000.

[9] Trapp, J and Ransom, V. *A Choked-Flow Calculation Criterion for Nonhomogeneous, Nonequilibrium, Two-Phase Flows.* International Journal of Multiphase Flow, 1982, pp. 669-681.

[10] Ishii, M. Argonne National Laboratory, private communication, letter to R. Nelson. July 1987.

[11] Los Alamos National Laboratory, Pennsylvania State University. *TRAC-M/FORTRAN 90 (VERSION 3.0) THEORY MANUAL.* Los Alamos, NM; University Park, PA, 2000. la-ur-00-910 edition.

[12] Ghiaasiaan, M. *Two-Phase Flow, Boiling, and Condensation in Vonventional and Miniature Systems.* New York : Cambridge University Press, 2008.

[13] Brennen, C. *Cavitation and Bubble Dynamics.* New York : Oxford University Press, 1995.

[14] Plesset, M and Zwick, S. *The Growth of Vapor Bubbles in Superheated Liquids.* Journal of Applied Physics, 1954, pp. 493-500.

Figure Captions

Fig. 1. Schematic of air shock tube.

Fig. 2. Pressure distribution in shock tube at 0, 5, and 10 ms.

Fig. 3. Model with location of pressure transducers and initial conditions.

Fig. 4. Thermal equilibrium simulation effect of time step at PT 3.

Fig. 5. Thermal equilibrium simulation effect of time step at PT 4.

Fig. 6. Thermal equilibrium simulation effect of time step at PT 5.

Fig. 7. Thermal equilibrium simulation sound speed (m/s) distribution with time.

Fig. 8. Thermal equilibrium simulation pressure (Pa) distribution with time.

Fig. 9. Thermal equilibrium simulation showing interaction of rarefaction wave with temperature gradient and subsequent voiding.

Fig. 10. Default simulation effect of time step at PT 3.

Fig. 11. Default simulation effect of time step at PT 4.

Fig. 12. Default simulation effect of time step at PT 5.

Fig. 13. 3D pressure plot using default simulation compared with experimental data (2).

Fig. 14. Default simulation sound speed (m/s) distribution with time.

Fig. 15. Default simulation sound speed (m/s) distribution at around 5 ms.

Fig. 16. Default simulation pressure (Pa) distribution with time.

Fig. 17. Initial pressure drop creating two-phase region and rarefaction wave reflection.

Fig. 18. Interaction of reflected rarefaction wave with temperature gradient.

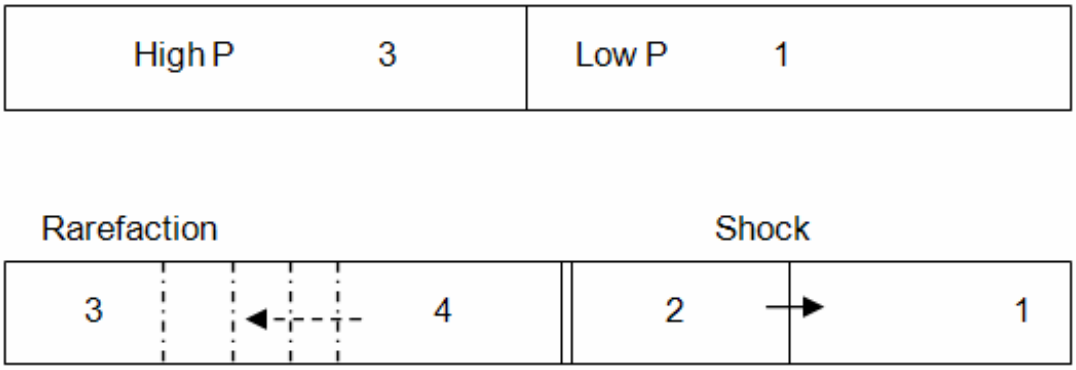

Fig. 1

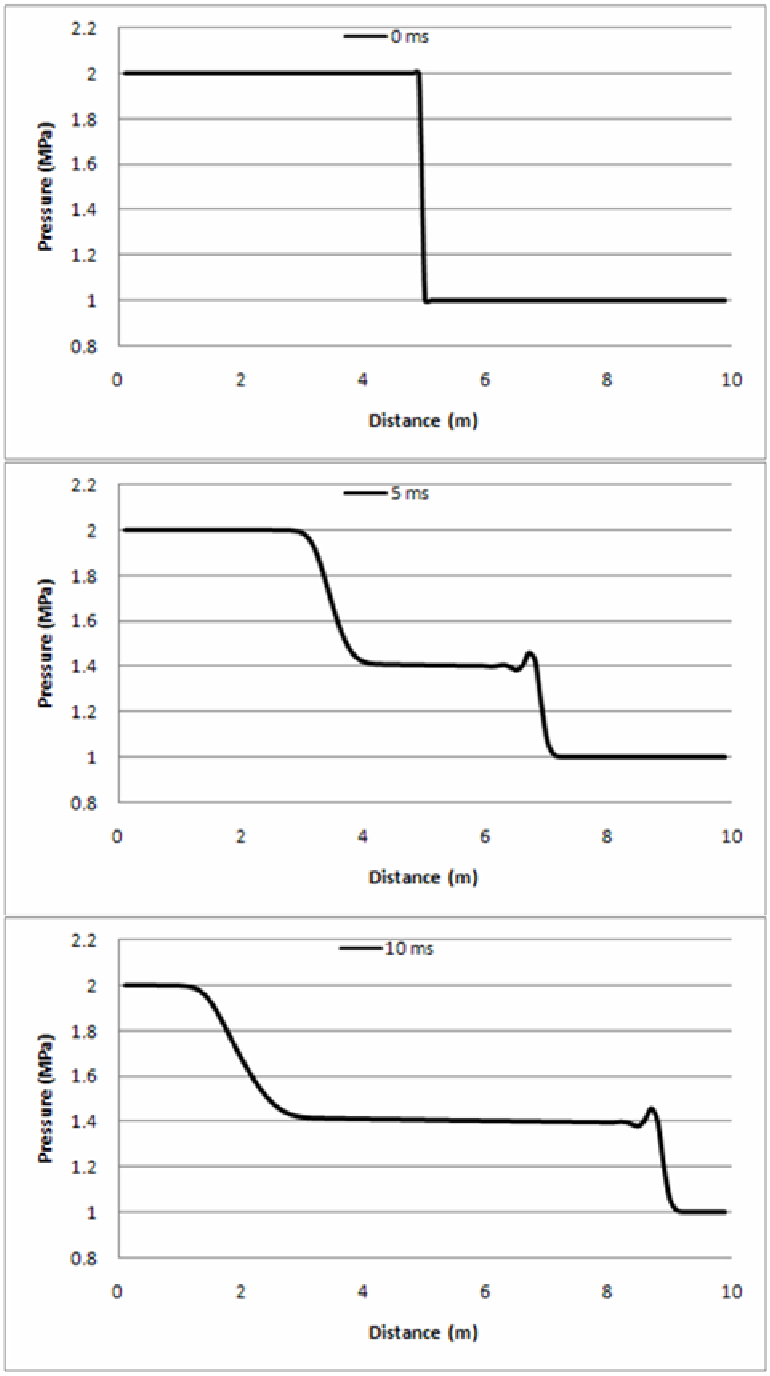
0 ms
Pressure (MPa)
2.2
2
1.8
1.6
1.4
1.2
1
0.8
0
2
4
6
8
10
Distance (m)
5 ms
Pressure (MPa)
Distance (m)
10 ms
Pressure (MPa)
Distance (m)

Fig. 2

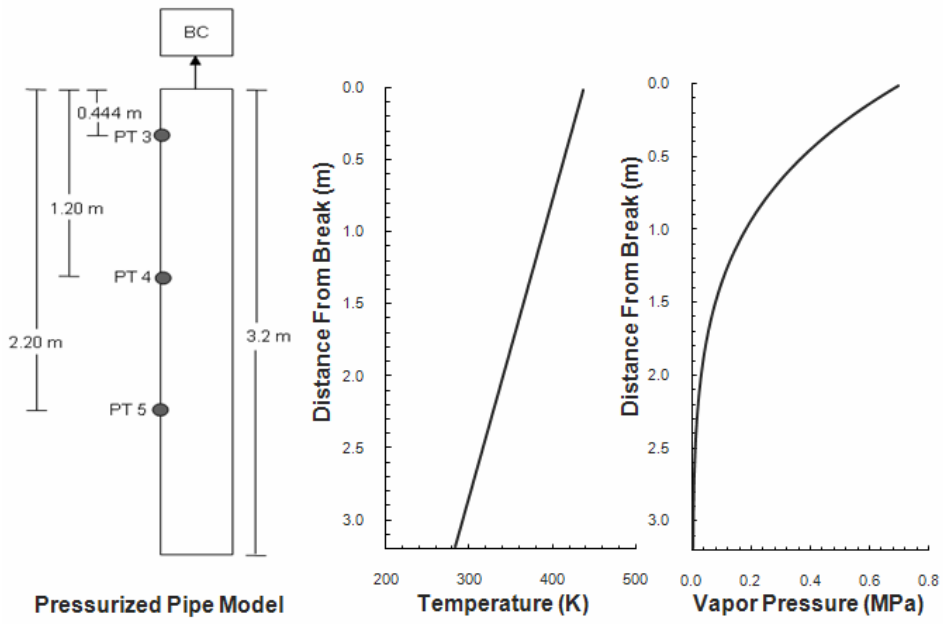
BC
0.444 m
PT 3
1.20 m
PT 4
2.20 m
3.2 m
PT 5
Pressurized Pipe Model
Distance From Break (m)
0.0
0.5
1.0
1.5
2.0
2.5
3.0
200
300
400
500
Temperature (K)
Distance From Break (m)
0.0
0.5
1.0
1.5
2.0
2.5
3.0
0.0
0.2
0.4
0.6
0.8
Vapor Pressure (MPa)

Fig. 3

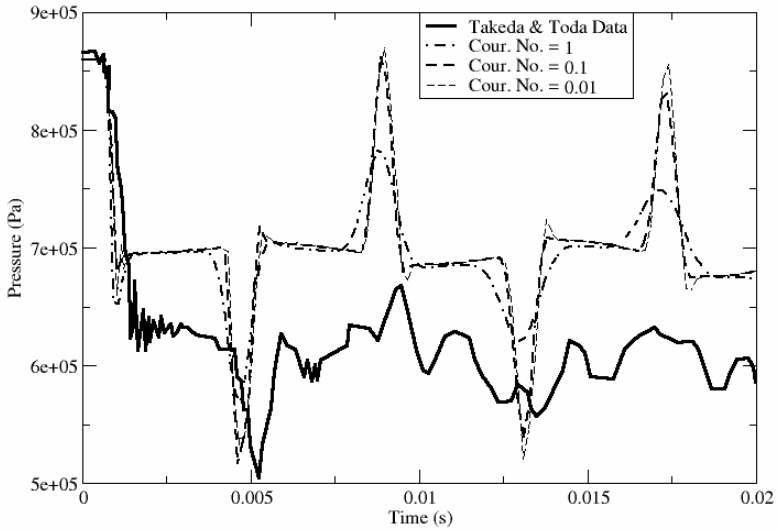
Takeda & Toda Data
Cour. No. = 1
Cour. No. = 0.1
Cour. No. = 0.01
Pressure (Pa)
Time (s)
9e+05
8e+05
7e+05
6e+05
5e+05
0
0.005
0.01
0.015
0.02

Fig. 4

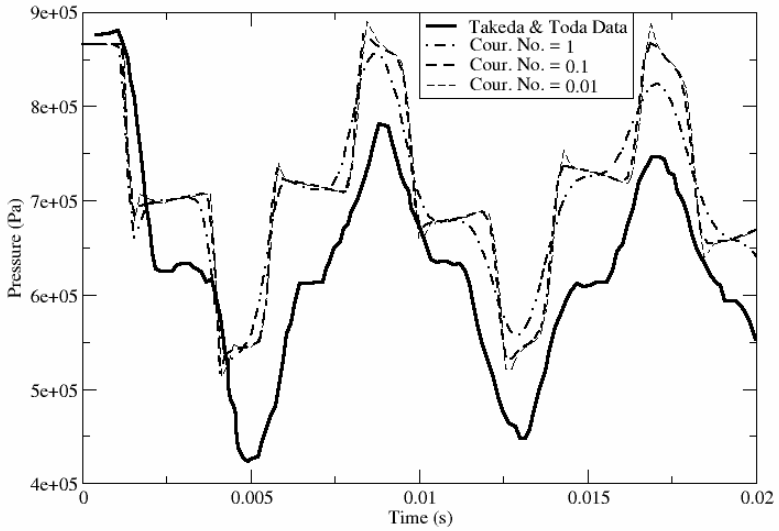
Takeda & Toda Data
Cour. No. = 1
Cour. No. = 0.1
Cour. No. = 0.01
Pressure (Pa)
Time (s)
9e+05
8e+05
7e+05
6e+05
5e+05
4e+05
0
0.005
0.01
0.015
0.02

Fig. 5

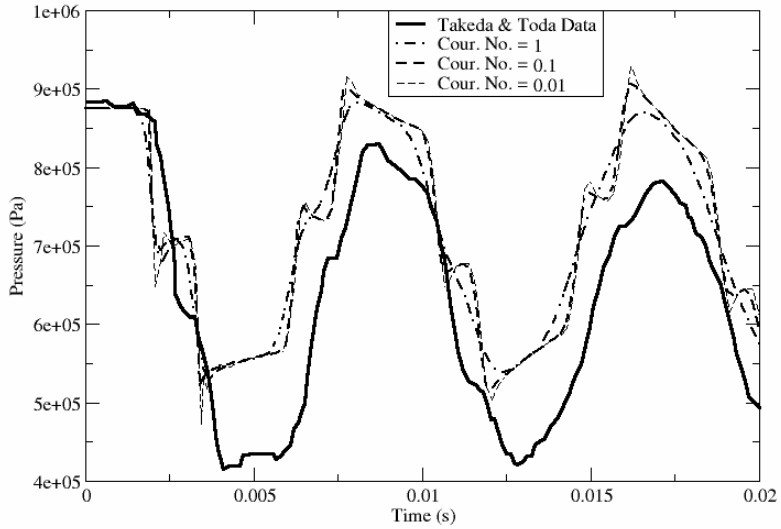
Takeda & Toda Data
Cour. No. = 1
Cour. No. = 0.1
Cour. No. = 0.01
Pressure (Pa)
Time (s)
1e+06
9e+05
8e+05
7e+05
6e+05
5e+05
4e+05
0
0.005
0.01
0.015
0.02

Fig. 6

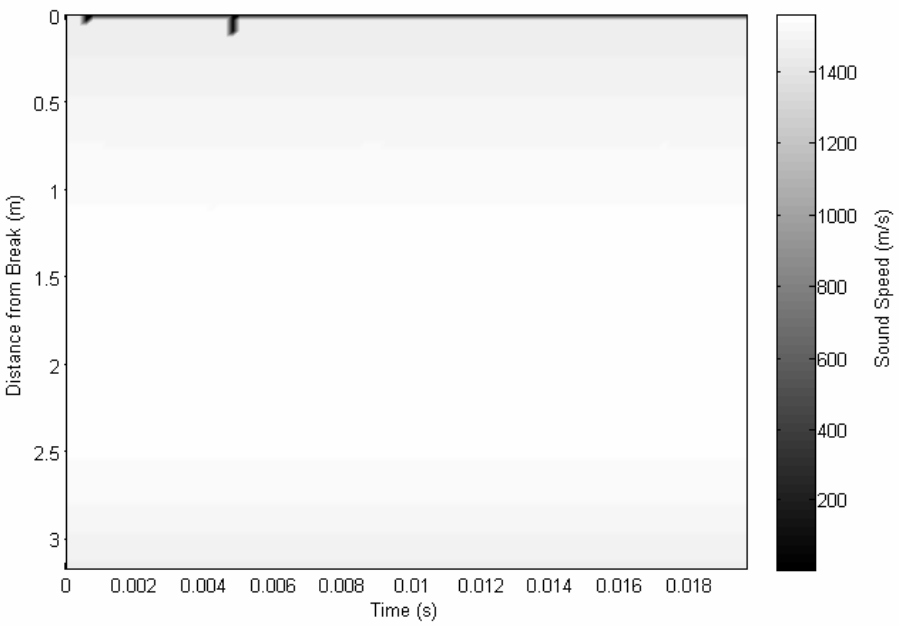
Distance from Break (m)
0
0.5
1
1.5
2
2.5
3
0
0.002
0.004
0.006
0.008
0.01
0.012
0.014
0.016
0.018
Time (s)
1400
1200
1000
800
600
400
200
Sound Speed (m/s)

Fig. 7

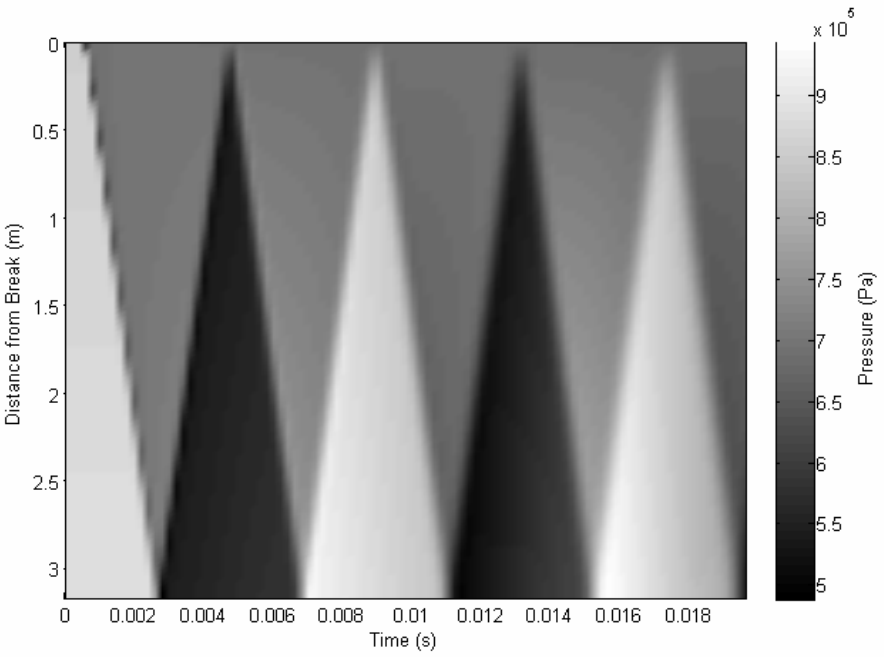
x 10^5
9
8.5
8
7.5
7
6.5
6
5.5
5
Pressure (Pa)
0
0.5
1
1.5
2
2.5
3
Distance from Break (m)
0
0.002
0.004
0.006
0.008
0.01
0.012
0.014
0.016
0.018
Time (s)

Fig. 8

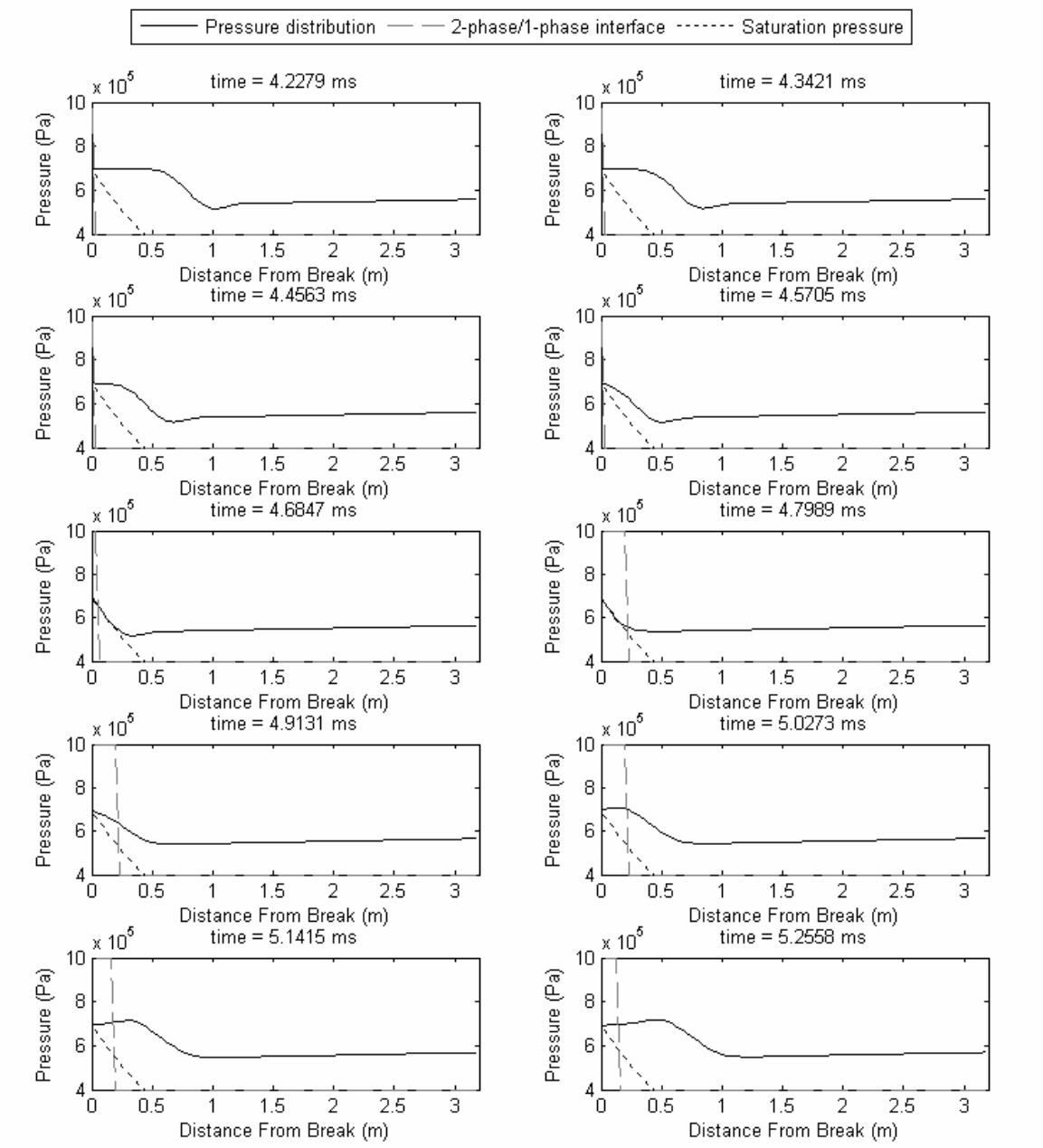
Pressure distribution
2-phase/1-phase interface
Saturation pressure
time = 4.2279 ms
time = 4.3421 ms
time = 4.4563 ms
time = 4.5705 ms
time = 4.6847 ms
time = 4.7989 ms
time = 4.9131 ms
time = 5.0273 ms
time = 5.1415 ms
time = 5.2558 ms
x 10^5
Pressure (Pa)
Distance From Break (m)

Fig. 9

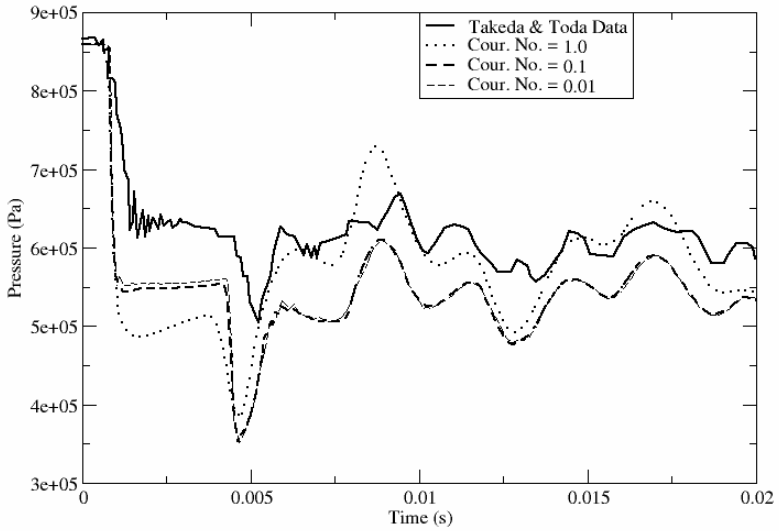
Takeda & Toda Data
Cour. No. = 1.0
Cour. No. = 0.1
Cour. No. = 0.01
Pressure (Pa)
Time (s)
9e+05
8e+05
7e+05
6e+05
5e+05
4e+05
3e+05
0
0.005
0.01
0.015
0.02

Fig. 10

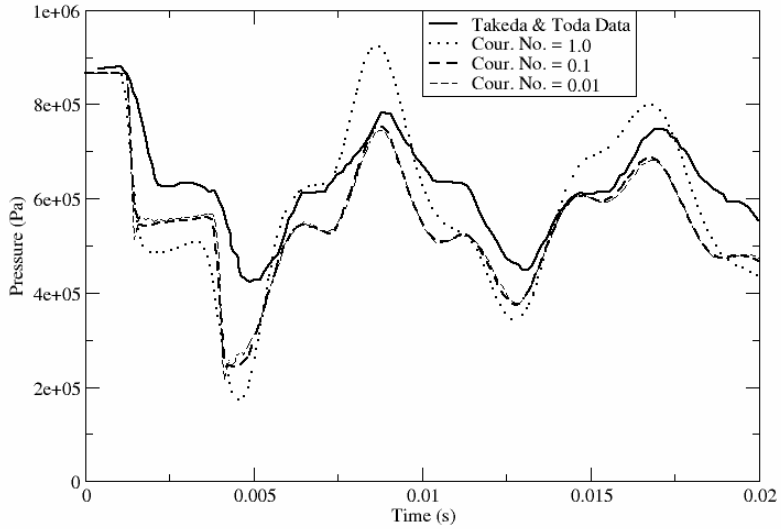
Takeda & Toda Data
Cour. No. = 1.0
Cour. No. = 0.1
Cour. No. = 0.01
Pressure (Pa)
Time (s)
1e+06
8e+05
6e+05
4e+05
2e+05
0
0
0.005
0.01
0.015
0.02

Fig. 11

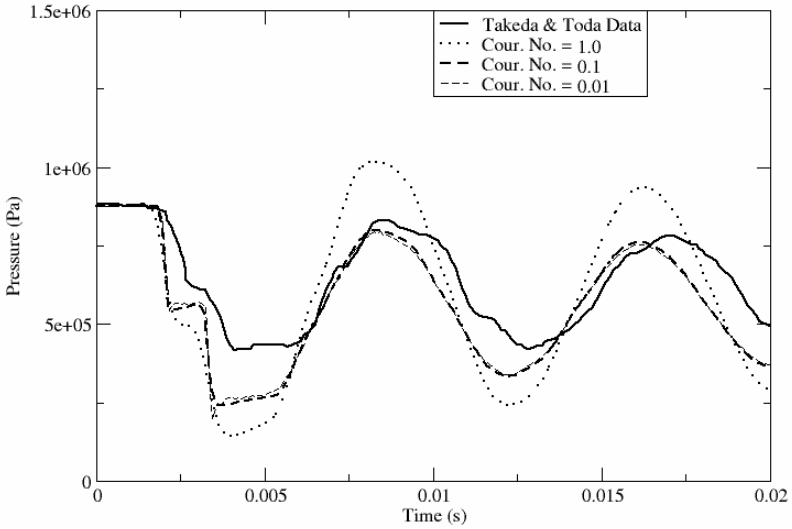
Takeda & Toda Data
Cour. No. = 1.0
Cour. No. = 0.1
Cour. No. = 0.01
1.5e+06
1e+06
5e+05
0
Pressure (Pa)
0
0.005
0.01
0.015
0.02
Time (s)

Fig. 12

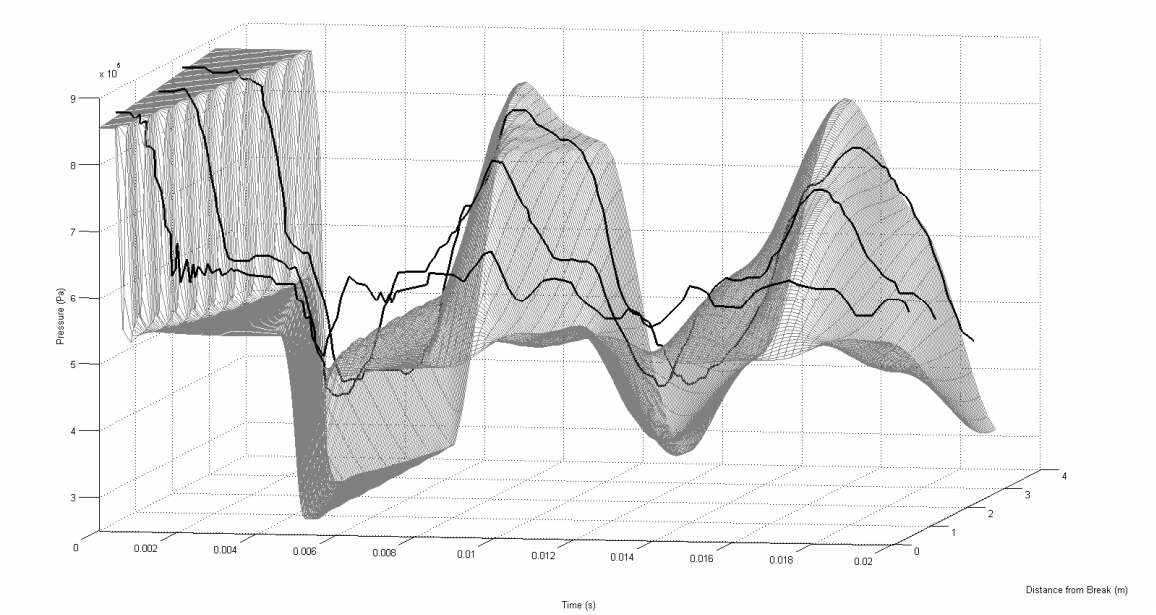
x 10^6
9
8
7
6
5
4
3
Pressure (Pa)
0
0.002
0.004
0.006
0.008
0.01
0.012
0.014
0.016
0.018
0.02
Time (s)
0
1
2
3
4
Distance from Break (m)

Fig. 13

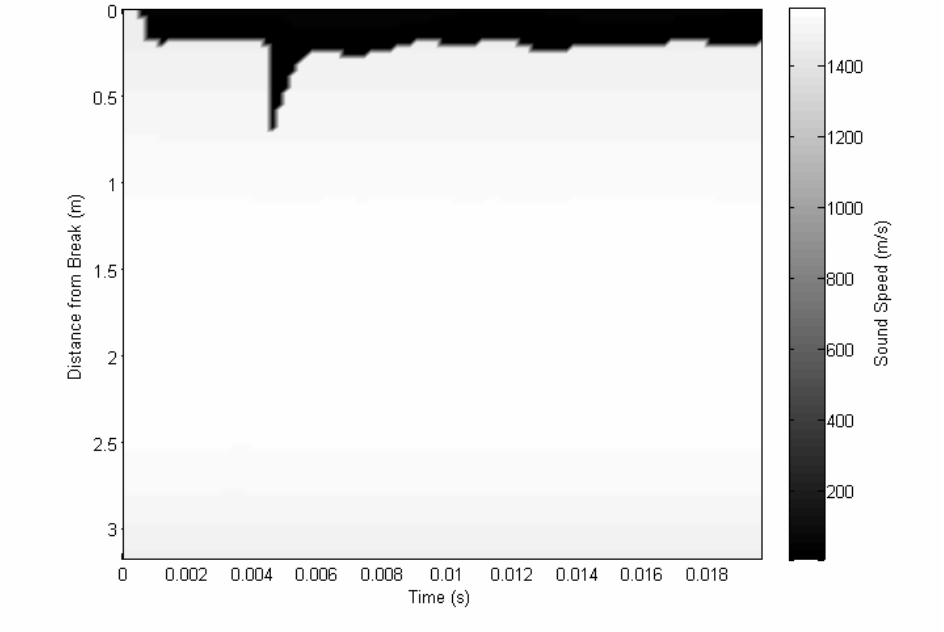
Distance from Break (m)
0
0.5
1
1.5
2
2.5
3
0
0.002
0.004
0.006
0.008
0.01
0.012
0.014
0.016
0.018
Time (s)
Sound Speed (m/s)
1400
1200
1000
800
600
400
200

Fig. 14

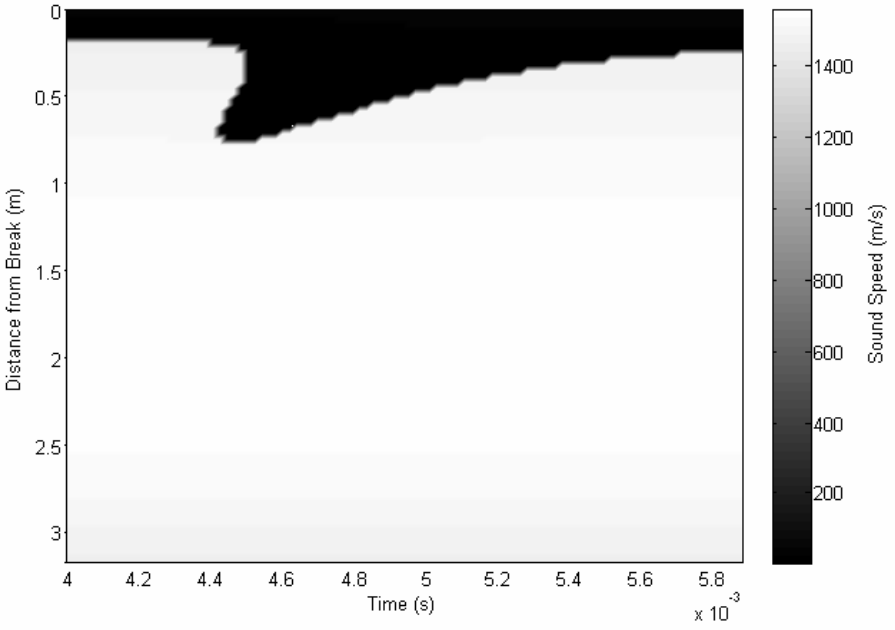
0
0.5
1
1.5
2
2.5
3
Distance from Break (m)
4
4.2
4.4
4.6
4.8
5
5.2
5.4
5.6
5.8
Time (s)
x 10^-3
1400
1200
1000
800
600
400
200
Sound Speed (m/s)

Fig. 15

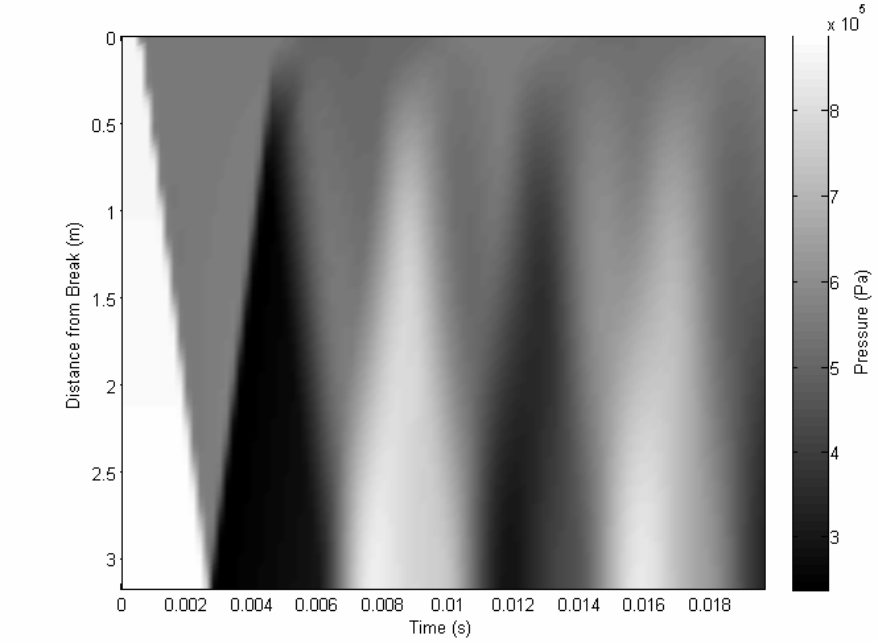
x 10^5
8
7
6
5
4
3
Pressure (Pa)
0
0.5
1
1.5
2
2.5
3
Distance from Break (m)
0
0.002
0.004
0.006
0.008
0.01
0.012
0.014
0.016
0.018
Time (s)

Fig. 16

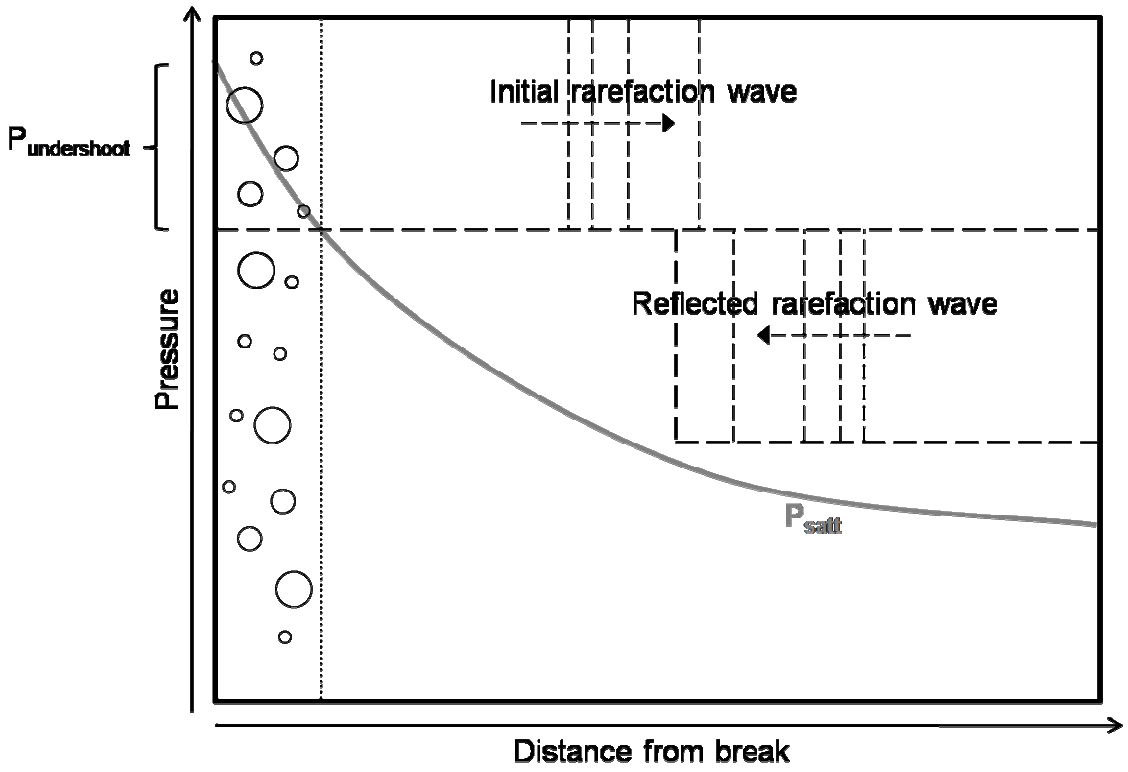
Initial rarefaction wave
P undershoot
Reflected rarefaction wave
Pressure
P satt
Distance from break

Fig. 17

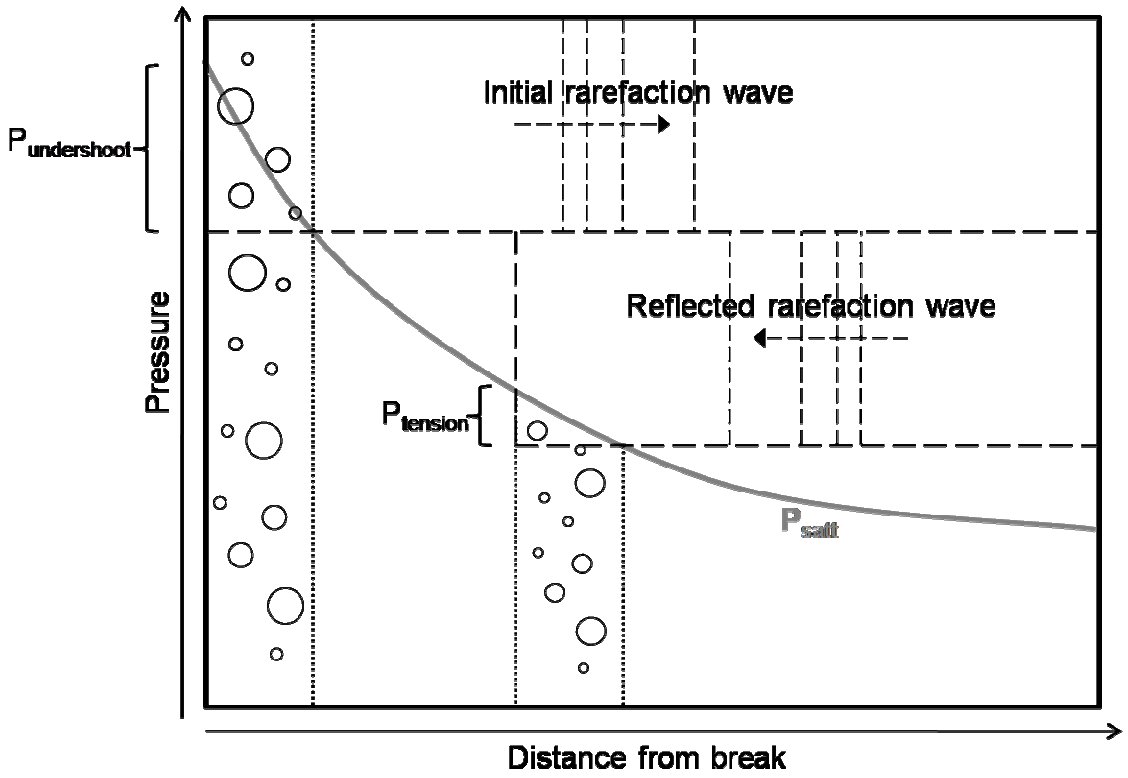
Initial rarefaction wave
Reflected rarefaction wave
P undershoot
P tension
P satt
Pressure
Distance from break

Fig. 18

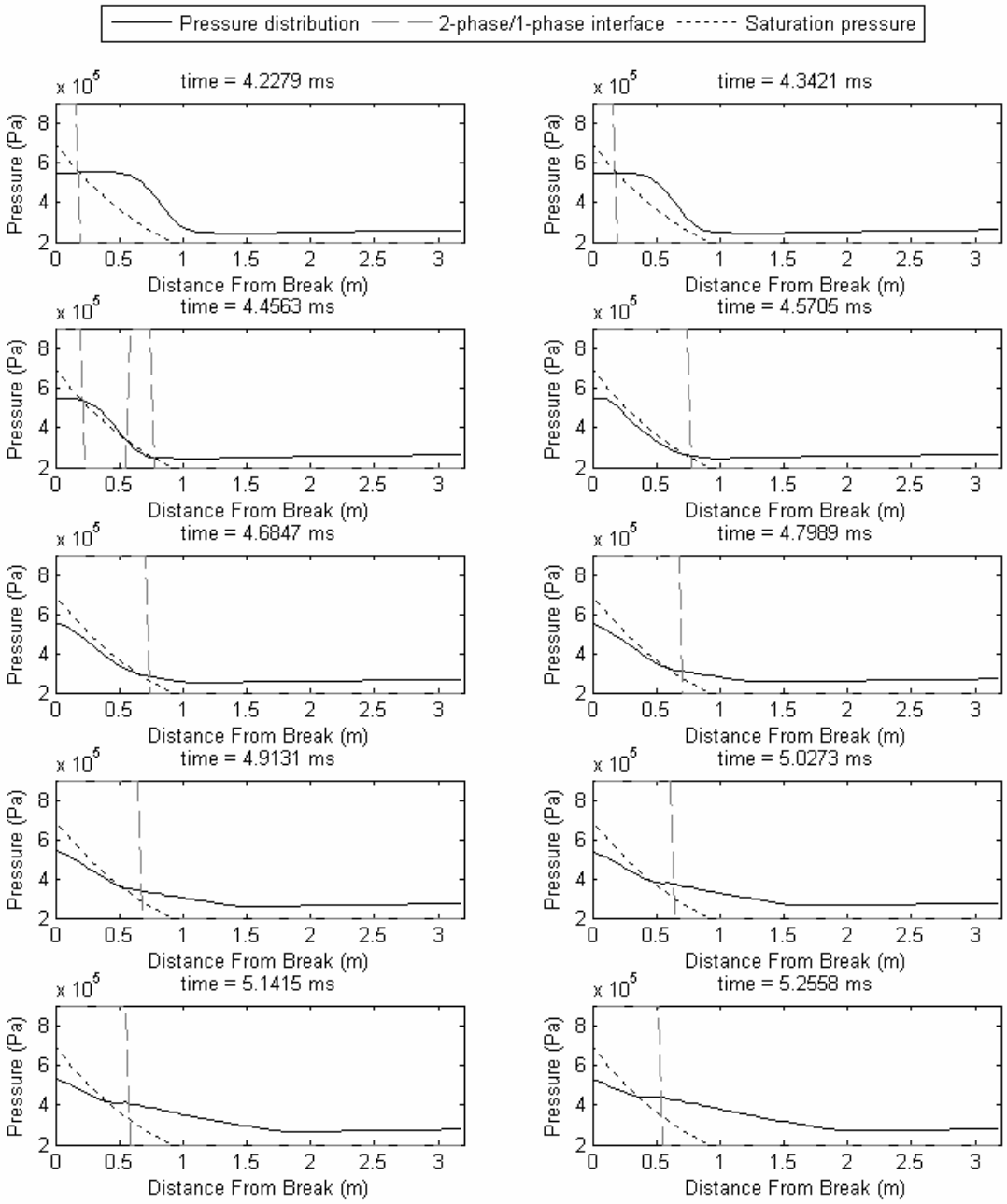
Pressure distribution
2-phase/1-phase interface
Saturation pressure
time = 4.2279 ms
time = 4.3421 ms
time = 4.4563 ms
time = 4.5705 ms
time = 4.6847 ms
time = 4.7989 ms
time = 4.9131 ms
time = 5.0273 ms
time = 5.1415 ms
time = 5.2558 ms
x 10^5
Pressure (Pa)
Distance From Break (m)

Fig. 19

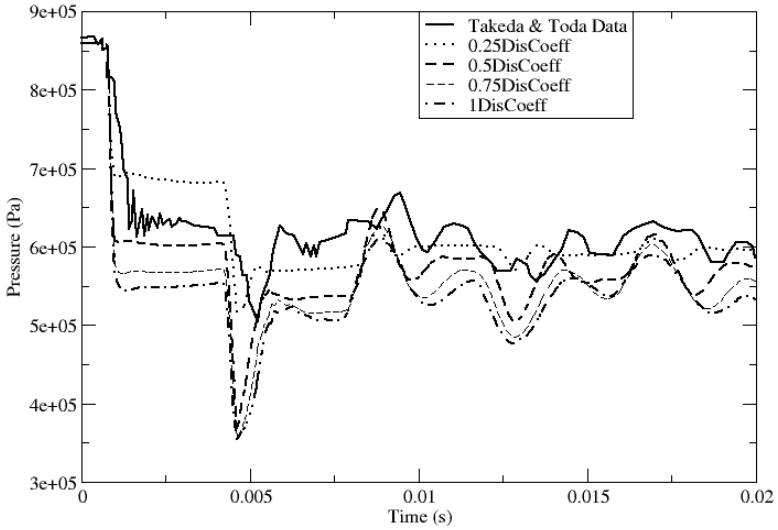
Takeda & Toda Data
0.25DisCoeff
0.5DisCoeff
0.75DisCoeff
1DisCoeff
Pressure (Pa)
Time (s)
9e+05
8e+05
7e+05
6e+05
5e+05
4e+05
3e+05
0
0.005
0.01
0.015
0.02

Fig. 20

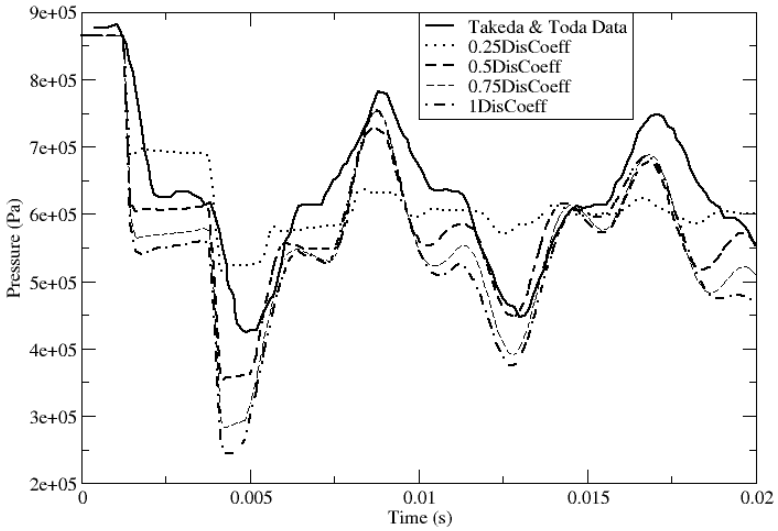
Takeda & Toda Data
0.25DisCoeff
0.5DisCoeff
0.75DisCoeff
1DisCoeff
Pressure (Pa)
Time (s)
9e+05
8e+05
7e+05
6e+05
5e+05
4e+05
3e+05
2e+05
0
0.005
0.01
0.015
0.02

Fig. 21

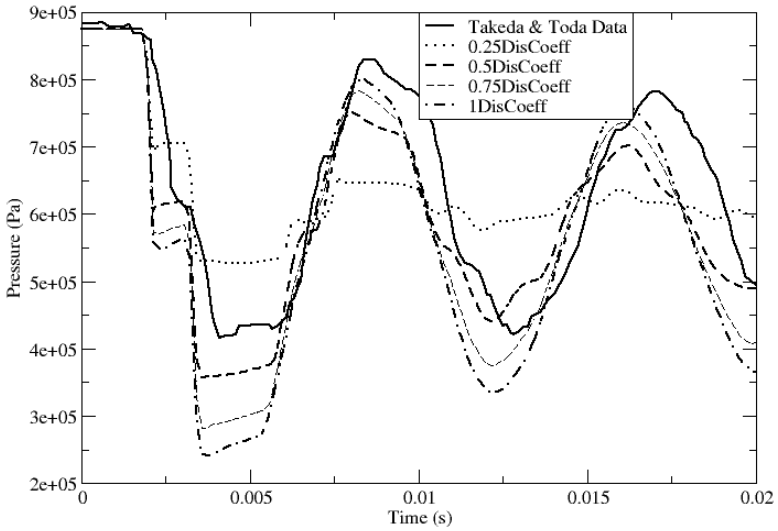
Takeda & Toda Data
0.25DisCoeff
0.5DisCoeff
0.75DisCoeff
1DisCoeff
Pressure (Pa)
Time (s)
9e+05
8e+05
7e+05
6e+05
5e+05
4e+05
3e+05
2e+05
0
0.005
0.01
0.015
0.02

Fig. 22

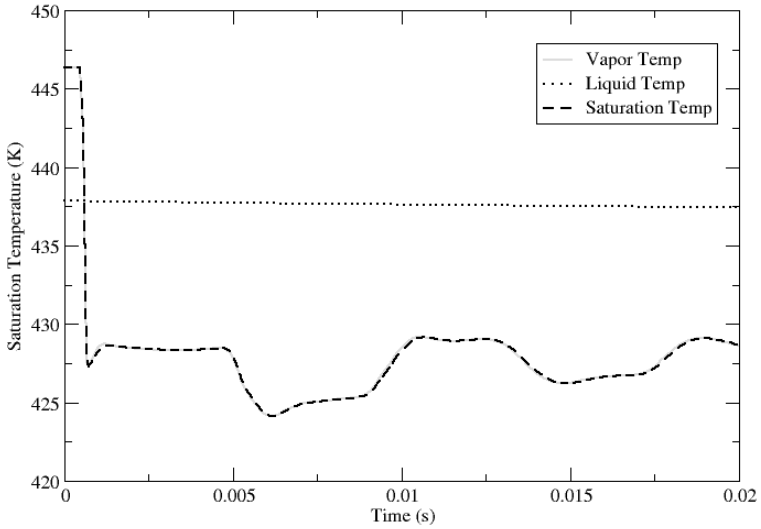
Vapor Temp
Liquid Temp
Saturation Temp
Saturation Temperature (K)
Time (s)
450
445
440
435
430
425
420
0
0.005
0.01
0.015
0.02

Fig. 23

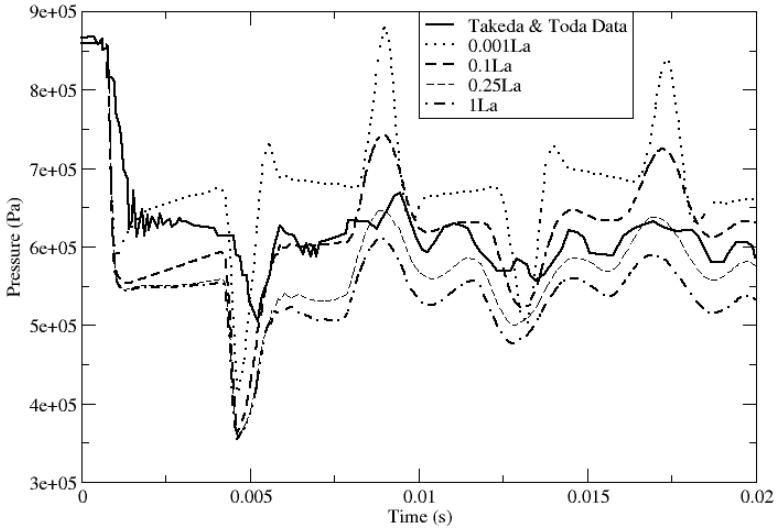
Takeda & Toda Data
0.001La
0.1La
0.25La
1La
Pressure (Pa)
Time (s)
9e+05
8e+05
7e+05
6e+05
5e+05
4e+05
3e+05
0
0.005
0.01
0.015
0.02

Fig. 24

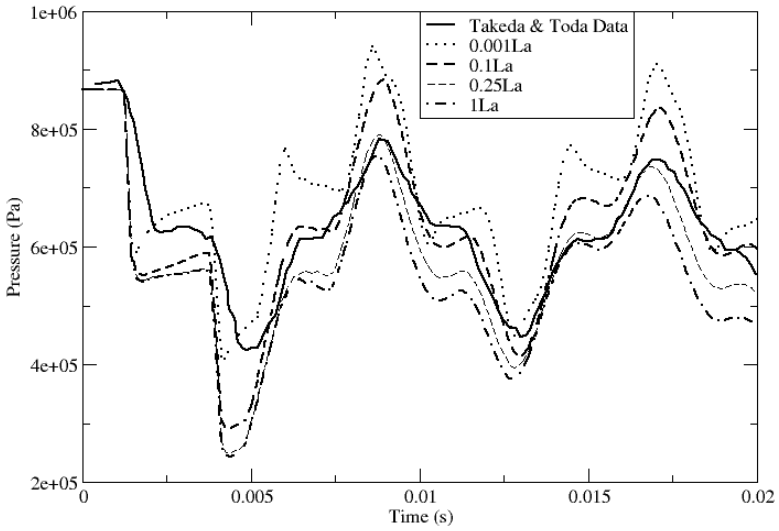
Takeda & Toda Data
0.001La
0.1La
0.25La
1La
1e+06
8e+05
6e+05
4e+05
2e+05
Pressure (Pa)
0
0.005
0.01
0.015
0.02
Time (s)

Fig. 25

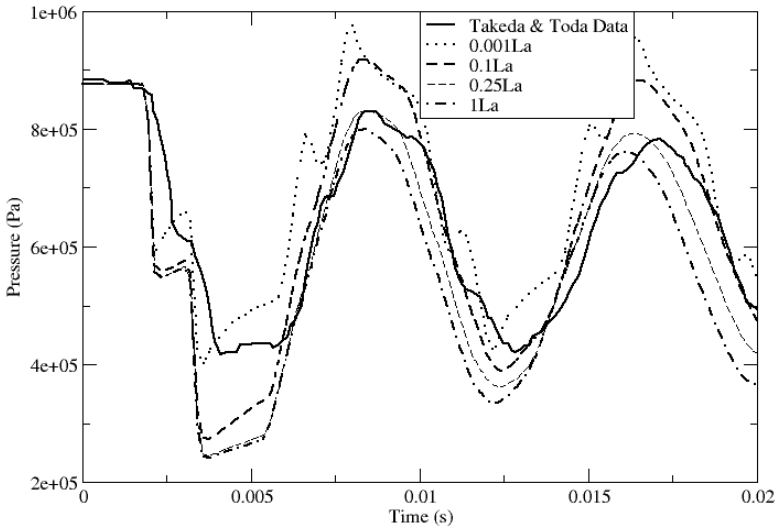
Takeda & Toda Data
0.001La
0.1La
0.25La
1La
1e+06
8e+05
6e+05
4e+05
2e+05
Pressure (Pa)
0
0.005
0.01
0.015
0.02
Time (s)

Fig. 26

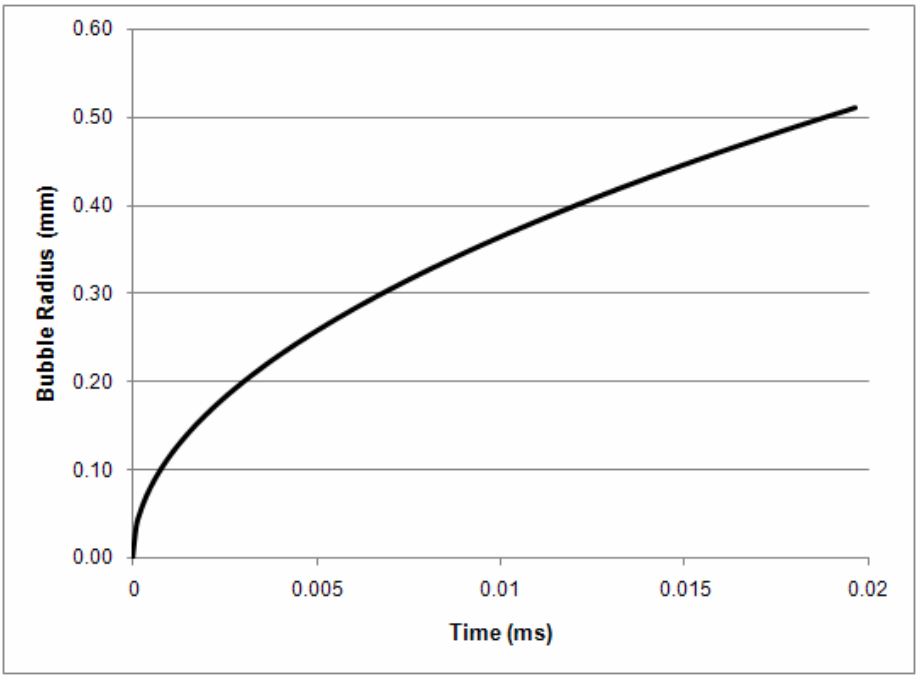
0.60
0.50
0.40
0.30
0.20
0.10
0.00
Bubble Radius (mm)
0
0.005
0.01
0.015
0.02
Time (ms)

Fig. 27

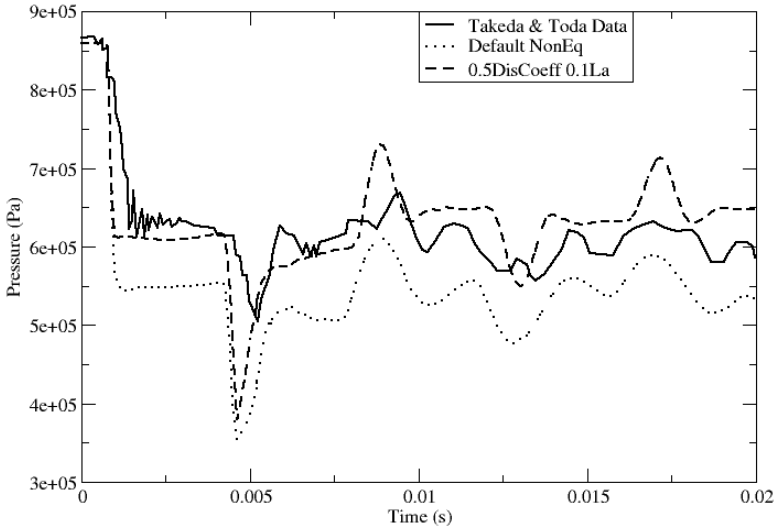
Takeda & Toda Data
Default NonEq
0.5DisCoeff 0.1La
9e+05
8e+05
7e+05
6e+05
5e+05
4e+05
3e+05
Pressure (Pa)
0
0.005
0.01
0.015
0.02
Time (s)

Fig. 28

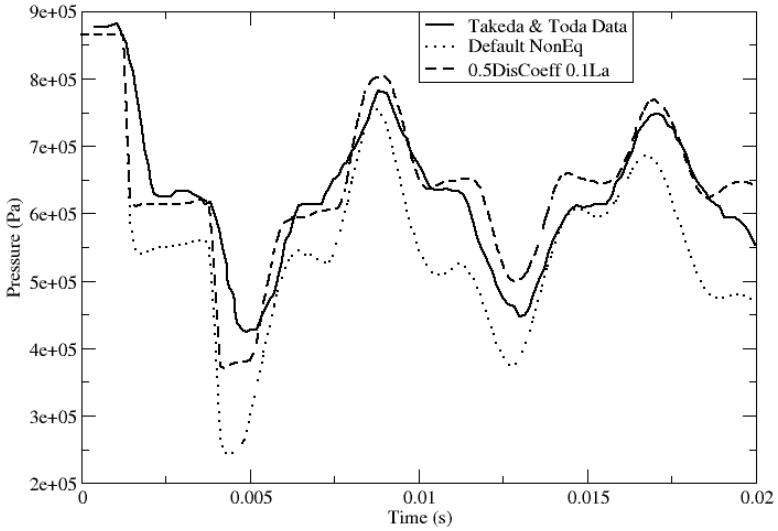
Takeda & Toda Data
Default NonEq
0.5DisCoeff 0.1La
Pressure (Pa)
Time (s)
9e+05
8e+05
7e+05
6e+05
5e+05
4e+05
3e+05
2e+05
0
0.005
0.01
0.015
0.02

Fig. 29

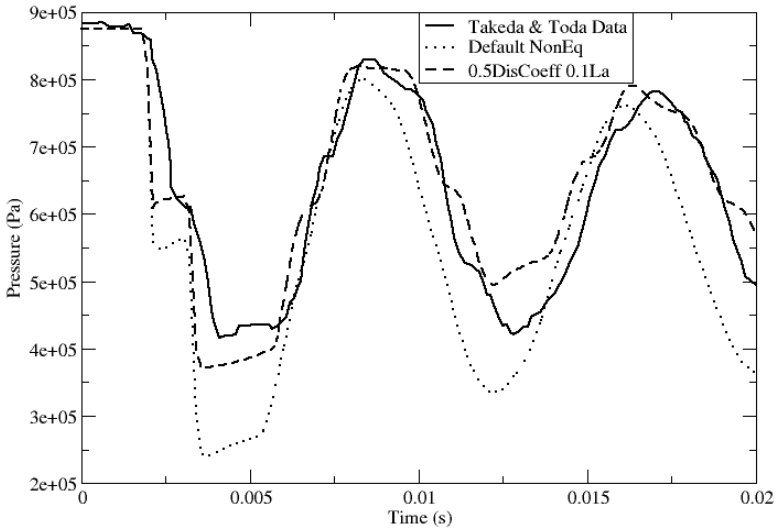
Takeda & Toda Data
Default NonEq
0.5DisCoeff 0.1La
Pressure (Pa)
Time (s)
9e+05
8e+05
7e+05
6e+05
5e+05
4e+05
3e+05
2e+05
0
0.005
0.01
0.015
0.02

Fig. 30

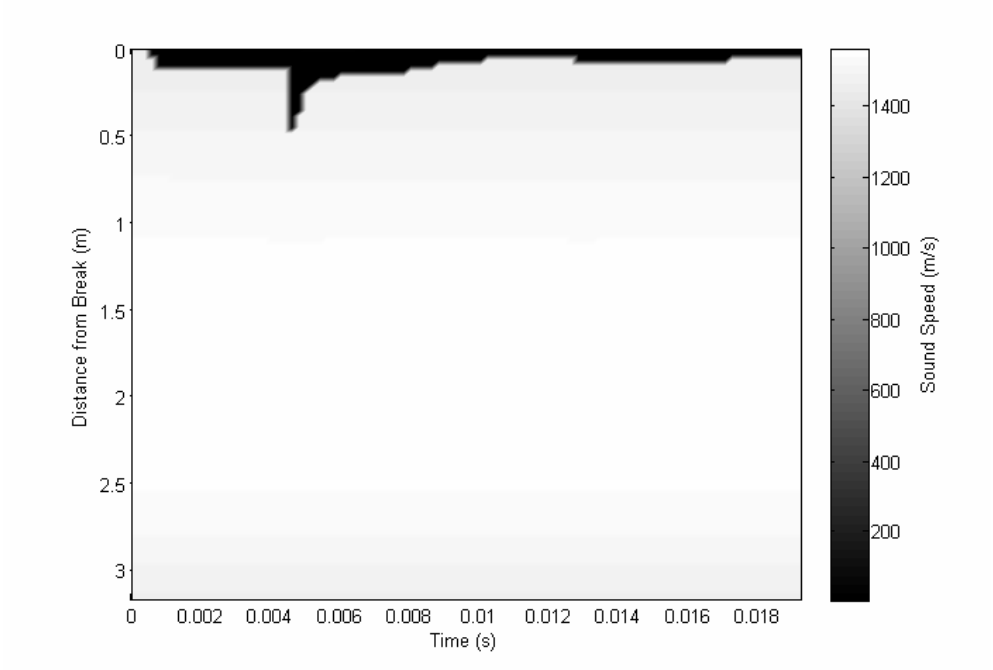
Distance from Break (m)
0
0.5
1
1.5
2
2.5
3
0
0.002
0.004
0.006
0.008
0.01
0.012
0.014
0.016
0.018
Time (s)
Sound Speed (m/s)
1400
1200
1000
800
600
400
200

Fig. 31

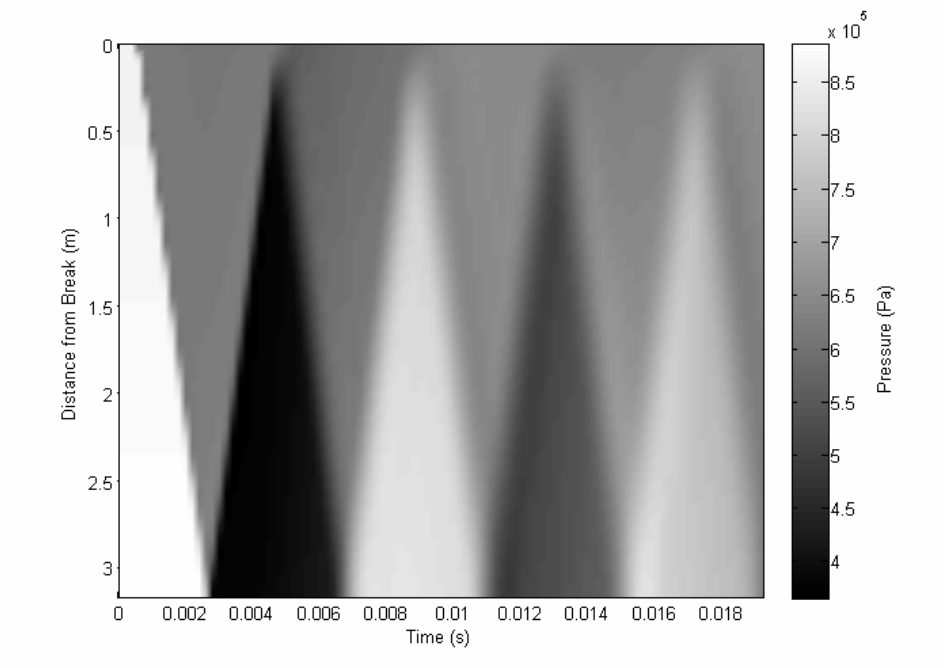
x 10^5
8.5
8
7.5
7
6.5
6
5.5
5
4.5
4
Pressure (Pa)
0
0.5
1
1.5
2
2.5
3
Distance from Break (m)
0
0.002
0.004
0.006
0.008
0.01
0.012
0.014
0.016
0.018
Time (s)

Fig. 32